UH 511-975-00

30 May 2001

Results from 3D silicon sensors with wall electrodes: near-cell-edge sensitivity measurements as a preview of active-edge sensors

Christopher J. Kenney, Sherwood Parker, and Edith Walckiers

Abstract—Silicon sensors with a three-dimensional architecture, in which the n and p electrodes penetrate through the entire substrate, have been successfully fabricated. The electrode spacing can be less than the substrate thickness, allowing short collection paths, low depletion voltages, and large current signals from rapid charge collection. This paper gives results when the cylindrical electrodes of the earlier papers are replaced by a combination of cylindrical and wall electrodes—ones in which a trench, rather than a hole, is filled with doped polycrystalline silicon. The detection efficiency remains high to within a few microns of these wall electrodes, and is an indication that similar high efficiencies should be achievable near the physical edges of the proposed active-edge sensors.

Index Terms—Active edges, insensitive edge regions, semiconductor sensors, silicon sensors, detectors, three-dimensional electrodes, 3D sensors, guard rings.

I. INTRODUCTION

Since the first custom VLSI chip was developed for the readout of silicon strip sensors [1], both the sensors and their readout chips have been fabricated by planar technology methods, in which all fabricated structures lie within a few microns of either surface. These sensors employ silicon diodes with electrodes in the form of closely spaced strips or pixels, with p-type electrodes on one surface and n-type ones on the other. Reverse-biased, they form a depleted diode with an electric field between the p and n electrodes for the collection of ionization charges. This field must be kept away from the saw cuts along the sensor edges, since they, with all their dangling bonds, are conducting and would short it out. Further space is needed to keep the field region from any cracks and chipped regions caused by the sawing. They can reach some tens of microns in from the edge. Space must also be left for guard rings, which drop the voltage in a controlled fashion, and intercept edge leakage currents before they reach the instrumented electrodes. For example, all these structures on the Atlas pixel sensors at CERN occupy 14% of the total surface area, not including any material in the saw lanes [2]. Figure 1 shows a schematic view of the various features that result in significant dead areas along sensor edges. Figure 2 shows an electron micrograph of a saw cut through four trenches. The sort of damage one must contend with, when saw cuts are used to separate sensors, is clearly visible in the photograph.

Silicon sensors having n-type and p-type electrodes that go from one surface, through the substrate, and end on the other surface, making a three-dimensional array, have been fabricated and tested [3], [4], [5], [6], [7]. They are fabricated using tools developed for micro-machining, which, together with the VLSI fabrication technology

from which it grew, are in combination, likely to have as large an impact on semiconductor detectors as did the original addition of custom VLSI readout chips.

Figure 3 shows a schematic view of part of a 3D sensor. This paper describes test results preliminary to the fabrication of the next new sensor type using 3D architecture: ones that are sensitive to within a micron or two of their physical edges. This will permit coverage of a large area with small, high-yield units that are tiled or placed in a shingled array without dead bands along their edges.

While this feature may only be desirable in many high-energy physics applications, where particles can penetrate many layers, it can be absolutely vital for some medical and biological uses. One proposed application, in the field of structural molecular biology, would make a high-rate, fast-readout, photon-counting detector for the diffraction patterns made by 12 KeV synchrotron x-rays that are scattered from protein crystals [8]. Measurement of the intensities of the Bragg spots, to an accuracy of about one percent, provides data that can be used for the determination of the three-dimensional structure of that protein—information that is required for a full understanding of its biological activity. This measurement cannot be done accurately if many spots overlap insensitive sensor edges.

II. PREVIOUS RESULTS

The first 3D paper, reference [3], described the planned fabrication methods and gave the results for calculations of expected depletion voltages, fields, charge motions, and expected pulse shapes. Reference [5] showed the first test results with fabricated sensors, gave details of the actual fabrication, and showed that, as expected, they had low depletion voltages. Reference [6] showed test results for sensors irradiated with 5×10^{14} 24 GeV, and 10^{14} to 10^{15} 55 MeV protons per cm^2, with the last one producing lattice damage equal to that expected after 10 years at the innermost B layer of the Atlas detector at CERN. Leakage currents, depletion voltages, release rates of trapped charge, and electrode capacitances were measured. (After the 10^{15} protons per cm^2 run, the sensor had a plateau, indicating full depletion of the silicon between the electrodes, and full charge collection from that volume, for bias voltages from 105 V to 150 V. This was with no beneficial annealing, and with no added oxygen in the silicon.) Reference [7] showed spectra from ^{241}Am and ^{55}Fe sources, in which mono-energetic lines are accurately fit with Gaussian shapes to ± 3s, with an approximately flat, low-side tail at a level of about 1-2% of the peak pulse height. The ^{241}Am 14.3 KeV line had a signal to noise ratio of 51 to 1.

III. PLANNED FABRICATION STEPS FOR ACTIVE EDGE SENSORS

As can be deduced from Figure 3, the electric field in 3D sensors will be parallel to the sensor surfaces, with corresponding points on the top and bottom having the same potential. The photomask that sets the electrode pattern for the holes can just as easily provide a trench around the border, and that trench can be filled with polycrystalline silicon at the same time the holes are filled. Unlike saw cuts, etched edges are quite smooth, and can provide a well-defined boundary, requiring only that the wafer be bonded to an underlying supporting wafer to hold the pieces of the sensor wafer together prior to the filling of the border trenches.

Detailed fabrication steps for the first 3D sensors are given in Table I of reference 5. Similar ones, with the addition of an etching step for a second set of trenches to dice the wafer, and a step to free the sensors from the support wafer at the end of the fabrication, could be used to produce active edge sensors. The major steps would then be:

1. Oxide-bond sensor wafer to support wafer.

2. Etch, dope, and fill holes for one type of electrode. (An alternate fabrication scheme, in which both types are etched and filled at the same time, then doped separately, is a possibility, but has not yet been tested.)

3. Etch, dope, and fill holes and border trenches for the other type. The trench width must be chosen so its vertical etch rate is close to that of the holes. Since both the fluorine, which does the etching, and the etching products can enter and leave trenches more easily, the width will normally be smaller than the hole diameter.

4. Heat to drive dopant atoms into single crystal silicon, including the silicon adjacent to the border trenches.

5. Deposit metal and pattern.

6. Etch dicing trenches. These will start within the active edge electrodes, leaving perhaps a micron or two of polycrystalline silicon to form a border around the single-crystal silicon. This forms a layer that protects the single-crystal silicon from mechanical damage and impurities. The dicing trench lithography, like all such steps, can be done with micron precision. The dicing trench etch will remove the rest of the border polycrystalline silicon from the adjacent sensors and the space between them.

7. Remove the supporting wafer and bonding oxide, using etching steps, thus separating the individual sensors.

Figure 4 shows a schematic view of the corners of two active edge sensors, prior to separation. The corners of a rectangular sensor are shown, but the process does not require any particular shape, which can be set by the needs of the experiment, and the requirements of the electrostatic field and the readout circuit. The top diagram shows the sensors after the holes and border trenches have been etched, doped and filled. The bottom diagram shows the sensors after the larger dicing trench (reaching to the dashed white lines in the top diagram) has been etched to separate the sensors.

IV. WALL ELECTRODE SENSORS

The masks for the first fabrication run were made before the support wafer technique was adopted, and so no active edge sensor designs were included. However ones with wall electrodes, alternating with the normal cylinder electrodes, were included. These wall electrodes, made by etching and filling trenches, use fabrication steps similar to those planned for active edge sensors.

Because of the important role active edge sensors could play in structural molecular biology and other fields of research requiring minimal sensor dead bands, we felt it would be useful to have a first look at the performance of already fabricated 3D sensors employing these wall electrodes.

The additional steps needed for active edge sensors, mainly the etching of the dicing trenches and the removal of the backing wafer, are done at relatively low temperatures, and would not be expected to change the dopant distributions, resultant electric fields, or sensor performance significantly. Both structures are expected to require that the electric fields end in the single crystal silicon, since the inter-crystal boundaries in the poly would be expected to be a source of large leakage currents. Consequently, it is expected that the near-edge-performance of active edge sensors should be similar to the near-cell-edge performance of sensors with wall electrodes, and thus can give a preview of active edge properties. Data in this paper is consistent with the region of high efficiency extending to within a few microns of the cell-bounding wall electrodes.

Since there is no bias field in the cylinder electrodes, to achieve full efficiency, their hole diameter must be small enough and/or the polycrystalline silicon used to fill the holes must have a minority carrier lifetime long enough to allow the diffusion of ionization charge made in the electrodes to a region of non-zero electric field. Alternately, it might be possible to replace the polycrystalline silicon with epitaxial (single crystal) silicon, matching the substrate lattice, in which case the collection field could extend into the electrodes. The sensors used for this paper occupy 1.2% of the volume of each pixel, and some of that should be insensitive. Work has started on both the trial fabrication of electrodes made with epitaxial silicon, and on attempts to narrow the electrode diameters.

V. WALL ELECTRODE TESTS—APPARATUS

Figure 5 shows a photomicrograph of the part of the sensor used for this paper. It had the wall and separately, the cylinder electrodes, joined with aluminum lines that led to probe pads, so a probe card could energize the entire sensor. The trench width on the mask was 5 µm, and the final width after etching was 11 µm. The cylinder diameter on the mask was 14 µm, and the final width was 19 µm. The aluminum traces above the trenches were 24 µm wide, and the aluminized circles on the cylinder electrodes had a diameter of 45 µm. The sensor thickness was the same as that used in references [4] – [7]: 121 µm.

Individual electrode measurements were made using a 12C Picoprobe, visible in the figure. It contacted a cylinder electrode that was isolated by cutting the aluminum trace to adjacent electrodes. The Picoprobe has an input resistance of 1 Megohm in parallel with a capacitance of 0.1 pF. Its output was recorded by a Tektronix TDS540 digital oscilloscope. A positive voltage was applied to the wall electrodes, and the cylinder electrodes, other than the one under measurement, were grounded. The voltage on that one differed from zero only by the (small) signal amplitude under measurement.

Tests were carried out using this setup, with an infrared micro-beam as a signal source. This was made by placing a Hewlett-Packard HFBR-1404 infrared light-emitting diode on

the center of the eyepiece of the Mitutoyo microscope on our Alessi probe station. The light-emitting diode had a wavelength of 820 nm, and a 1/e penetration depth of about 14 μm in silicon. The spot diameter on the sensor could be varied by the selection of either a 2x, 10x, 20x, 50x, or 100x objective lens together with a 1x—2x zoom. Spot sizes of 30 and 300 μm were used for the measurements in this paper.

VI. WALL ELECTRODE RESULTS—DEPLETION VOLTAGE

Figure 6 shows full depletion and full charge collection onto a strip of 12 joined p-type cylinder electrodes at 15 V and possibly a few volts lower. Figure 7 shows full depletion and charge collection on a single p-type cylinder electrode from its 75 μm x 320 μm cell at about 10 - 12 V. Capacitance measurements, described in section VIII, also indicate full depletion occurs in the 8 – 10 V region. Leakage currents were also measured, and were in the nanoamp range, comparable to those in other 3D devices, such as those shown in Figures 15 and 16 of reference [5].

The slightly higher bias voltages required for full signal heights, compared with those of references [5] and [6], while still low compared with those needed for typical planar sensors, is due to the greater width of the wall electrode cells. The slight decrease in signal at higher bias voltages is due to the aluminum traces, visible in Figure 5, inverting the underlying silicon, and making a conducting channel that intercepts a small part of the signal charge.

For these measurements, a 10x objective was used with the zoom set at 1x, producing a spot that was centered on the electrode being probed, and that should be 10 times larger than the 30 μm spot whose size measurement is described below. This is slightly less than the 320 μm width of the cell. However, since the substrate is p-type, the depletion zone starts at the edges of the illuminated region next to the n-type wall electrodes, and expands to its final size by extending to the cylinder electrode in the center of the illuminated region, so the signal should increase until the depletion zone reaches the volume under the aluminum, a bit over 10 μm from the edge of the heavily doped single crystal silicon around the poly electrode.

VII. WALL ELECTRODE RESULTS—SMALL-SPOT SCANS

Figure 8 shows the signal when the microscope is moved in the y direction, parallel to the wall electrodes, as indicated by the line in Figure 5. For these measurements, a small spot is desired, rather than one that illuminates an entire cell, so the 50x objective was used with the zoom set at 2x.

The rise in signal amplitude on the left side of the graph occurs as the full infrared spot crosses the lower electrostatic boundary halfway between the probed electrode and the one below it in Figure 5. The microscope motion to produce that change, 30 μm, gives the effective spot width, including any broadening due to the variation of the width with depth. The initial decline in amplitude on the right side of the plot at about 67 μm, occurs when the left side of the spot lands on the probe needle rather than the sensor, and before the microscope motion brings top of the spot to the upper electrostatic boundary. In the absence of obscuring features such as that needle and the aluminum traces on the silicon, the full width at half-max would correspond to the microscope motion needed

to translate the line dividing the spot into two equal intensity halves from the upper to the lower electrostatic boundary. The measured value, 73 μm, is not far from the expected 75 μm. The measured value of the full width of the pattern, 108 μm, is also not far from the expected value of the spot size plus the electrode pitch, 30 μm + 75 μm = 105 μm.

The amplitude dependence for the x direction scan, perpendicular to the wall electrodes (along the other line in Figure 5) is shown in Figure 9. It is a bit more complex. The infrared spot crosses, and is absorbed by (from left to right on the graph, and from right to left in the photograph), the aluminum over the wall electrode, the aluminum trace to its left, the aluminum of the probed cylinder electrode, the trace leading to the two cylinder electrodes at the top of the figure, and finally, the aluminum of the left wall electrode. The dips in signal intensity occur at the expected locations, and the measured full width at half max, 287 μm, is close to the expected 290 μm. (An extra aluminum trace, adjacent to the aluminum over the trench and visible to the left of the right trench in Figure 5, further narrows the illuminated region.)

For reasons similar to those applying to the y direction scan, when the midpoint of the illumination pattern crosses the border of the aluminum, the signal would be expected to drop to half of its maximum value, providing any spread of the pattern above or below the focal plane did not result in light reaching insensitive silicon. Thus, the agreement between the predicted and observed pattern widths to within 3 μm means we have verified sensitivity to within 1.5 μm or less from each aluminum border. On the side without the extra trace, that border is (24 – 19)/2 μm = 2.5 μm from the poly electrode, and somewhat less from the heavily doped and so undepleted single crystal silicon.

VIII. WALL ELECTRODE RESULTS—CAPACITANCE

The signal amplitude can also be used to measure the capacitance of the probed electrode, since the leakage currents are much smaller than these signal currents. In addition, many infrared pulses are averaged using the digital oscilloscope. For this measurement, the pulse to the infrared diode is turned off. After the diode stops emitting and the last of the charge is collected, the signal shows a pure RC exponential fall. Reference [6] shows many such plots for sensors with cylinder electrodes at both diode terminals. Figure 10 similar exponentials for the wall—cylinder sensors studied here, and Figure 11, the derived RC times, as a function of the bias voltage. At and above 8 volts, the RC time is about 330 ns. Dividing by R_{probe} and subtracting C_{probe} gives an electrode capacitance of 0.23 pF, only slightly larger than 0.20 pF for the capacitance of the electrodes of reference [6]. (Like-type cylinder electrodes there were also aligned in columns, but with a pitch of 100 rather than 75 μm, and were separated by 100 μm from the columns of unlike electrodes. The positions of the two sets of electrodes in the column (y) direction were staggered by 50 μm, maximizing their separations.)

IX. CONCLUSIONS

Devices have been fabricated with the key elements that will be needed for active edge sensors: wall electrodes combined with cylinder electrodes. The cylinder electrodes have capacitances comparable to those of 3D sensors using cylinder electrodes only. The sensors have low leakage currents, signal plateaus at voltages that are comparable

to those reported for cylinder electrode 3D devices, and a sensitive volume whose border is less than 4 μm from the wall electrode edges.

ACKNOWLEDGEMETS

We would like to thank C.Storment and J. McVittie, who provided valuable information and advice, Julie Segal who devised the initial fabrication steps and performed many calculations, A. Partridge, who allowed us the use of the wafer bonding apparatus, the staff of the Stanford Nanofabrication Facility who provided continuing help in very many ways, and J. Plummer and H. Yamamoto for their interest and support. The work was supported by the U.S. Department of Energy under grant DE-FG03-94ER40833. We also appreciate the funding of the Stanford Nanofabrication Facility by the National Science Foundation. We have received vital help in the form of computer support and office space from the Stanford Linear Accelerator Center and the Lawrence Berkeley Laboratory.

REFERENCES

[1] J. Walker, S. I. Parker, B. Hyams, and S. Shapiro, "Development of high density readout for silicon strip detectors", *Nucl. Instr. and Meth*. A 226 (Sept. 1984) 200-203.

[2] M. S. Alam, et al., “The Atlas silicon pixel sensors”, CERN report ATLAS-INDET-99-012, 10 Sept. 1999, pp 1,2.

[3] S. Parker, C. J. Kenney, and J. Segal, "3D--A proposed new architecture for solid-state radiation detectors", *Nucl. Instr. and Meth*. A 395 (Aug. 1997) 328-343.

[4] C. J. Kenney, S. I. Parker, J. Segal, and C. Storment, "Comparison of 3D and planar silicon detectors", *Proceedings of the 9th meeting of the Division of Particles and Fields of the American Physical Society*, Minneapolis, MN, 11-15 Aug. 1996, World Scientific, 1998, vol. 2, pp. 1342-1345.

[5] C. J. Kenney, S. I. Parker, J. Segal, and C. Storment, “Silicon detectors with 3-D electrode arrays: fabrication and initial test results”, *IEEE Trans. Nucl. Sci.* 46 (1999) 1224 – 1236.

[6] Sherwood I. Parker and Christopher J. Kenney, “Performance of 3D architecture, silicon sensors after intense proton irradiation”, U. of Hawaii preprint UH 511-959-00, August 2000, submitted for publication.

[7] Christopher J. Kenney, Sherwood I. Parker, Brad Krieger, Bernhard Ludewigt, Tim Dubbs, and Hartmut Sadrozinski, “Observation of beta and X rays with 3D-architecture, silicon micro-strip sensors”, *IEEE Trans. Nucl. Sci,* 48 (2001) 189 - 193.

[8] E. Westbrook, S. Parker, and C. Kenney, “3DX: A Micromachined silicon crystallographic X-ray Detector”, NIH Proposal 1R01RR16230-01, 29 Sept. 2000.

S. Parker is with the University of Hawaii, Honolulu, HI 96822, (email: sher@slac.stanford.edu)
C. Kenney was with the University of Hawaii. He is now with MuSquared, Inc., 3061B Zanker Rd., San Jose, CA 95134.
E. Walckiers is now with Philips Semiconductors AG, Binz 44, CH-8045, Zurich, Switzerland

FIGURE CAPTIONS

1. Schematic cross section view of a sensor edge, showing some reasons for the insensitive region there: (a) space may be needed for guard and voltage-dropping rings, (b) the saw-cut edges are conducting, and (c) often contain chips or micro-cracks, all of which must remain clear of (d), the bulge of the edge of the electric field in the depleted region.

2. Photograph of the cross section of a 525 µm-thick wafer with etched trenches. Damage from the diamond saw wheel, schematically indicated in Fig. 1 can be seen along the right center and left surfaces.

3. Schematic three-dimensional view of part of a sensor with 3D electrodes penetrating the substrate. The front border of the figure is drawn through the center of three electrodes.

4. Schematic view of part of two adjacent active edge detectors still bonded, with an oxide layer, to their support wafer (not to scale). The top diagram shows the sensors after the holes and trenches for the n and p electrodes have been etched, doped and filled. The bottom diagram shows the sensors after the larger dicing trench (reaching to the dashed white lines in the top diagram) has been etched to separate the sensors. The visible parts of the doped polycrystalline silicon electrodes are shaded, with the lighter shading on the vertical sensor edge faces just used for clarity. Metal lines are not shown. The right-side cut face (dashed lines) shows a schematic view of the interior.

5. Photomicrograph of part of a sensor with alternating n-type wall and p-type cylinder electrodes and with electrodes tied together with aluminum traces, so the entire sensor can be energized with the limited number of probes available on one of our probe cards. The central cylinder electrode in the figure has been isolated, and is then kept near ground potential by the 1 Megohm input resistance of a 12C Picoprobe. The probe tip can be seen on the electrode, with its upper part (mostly out of focus) slightly to the right of the electrodes. The wall-to-wall electrode pitch is 320 µm, and the cylinder-to-cylinder pitch is 75 µm. The as-drawn width of the trenches on the lithographic mask used to etch them was 5 µm; the actual width of the etched trenches that were filled to make the wall electrodes was 11 µm. The as-drawn diameter of the holes on the mask was 14 µm; the actual diameter of the holes was 19 µm. The scan lines for the infrared spot traversals of Figures 8 and 9 are indicated by the lines labeled "Y-scan" and "X-scan".

6. Signal voltage from a strip of 12 p-type cylinder electrodes, when an entire cell is illuminated by an infrared diode micro-beam, as a function of the voltage on the wall electrodes.

7. Signal voltage from a single p-type cylinder electrode, when its entire cell is illuminated by an infrared diode micro-beam, as a function of the voltage on the wall electrodes.

8. Signal voltage from a single p-type cylinder electrode, illuminated by a small-diameter infrared micro-beam, as the beam is scanned in the y direction (parallel to the wall electrodes). The line is drawn to link all the points for greater clarity.

9. Signal voltage from a single p-type cylinder electrode, illuminated by a small-diameter infrared micro-beam, as the beam is scanned in the x direction (perpendicular to the wall electrodes).

10. Signal voltages from a single p-type cylinder electrode and least squares linear fits for four values of bias voltage: crosses and solid line (5V), circles and dotted line (6V), diamonds and dashed line (8V), and squares and dot-dashed line (40V). The signal came from an infrared micro-beam which was turned off at time = 0. The exponential RC decay time is set by the 1 Megohm input resistance of the Picoprobe multiplied by the sum of its 0.1 pF input capacitance plus the capacitance of the cylinder electrode. Individual RC values can be seen in the next figure.

11. Plot of RC times from Figure 11 as a function of applied voltage.

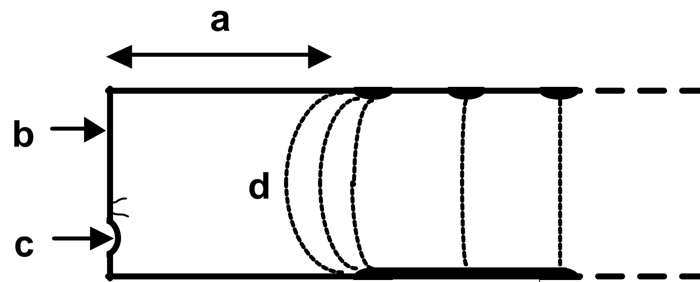
a
b
c
d

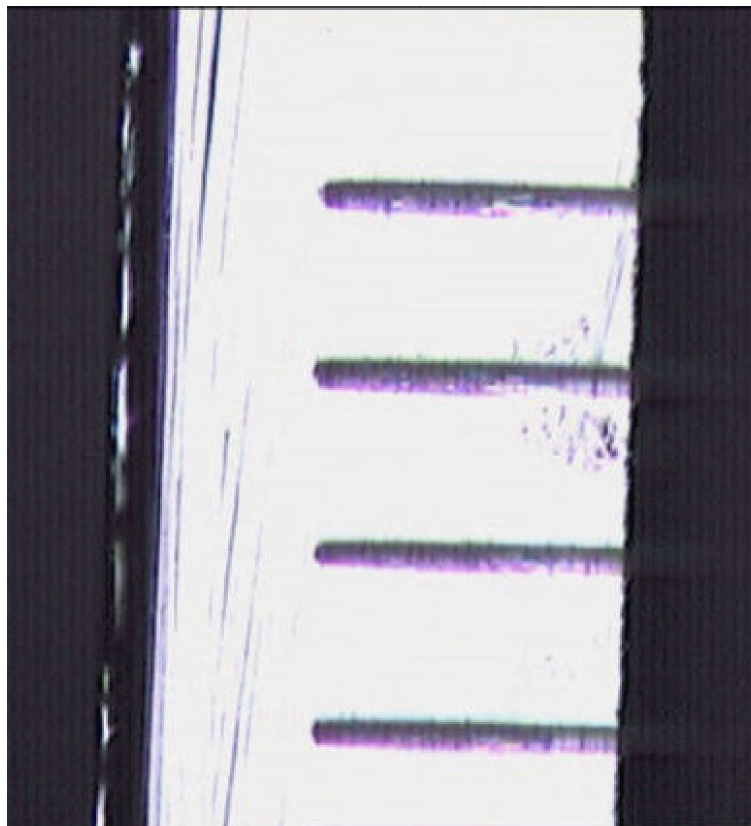

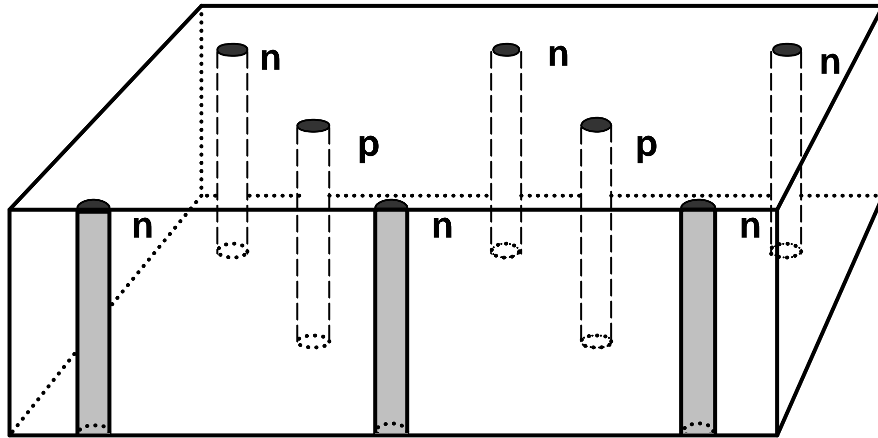
n
n
n
p
p
n
n
n

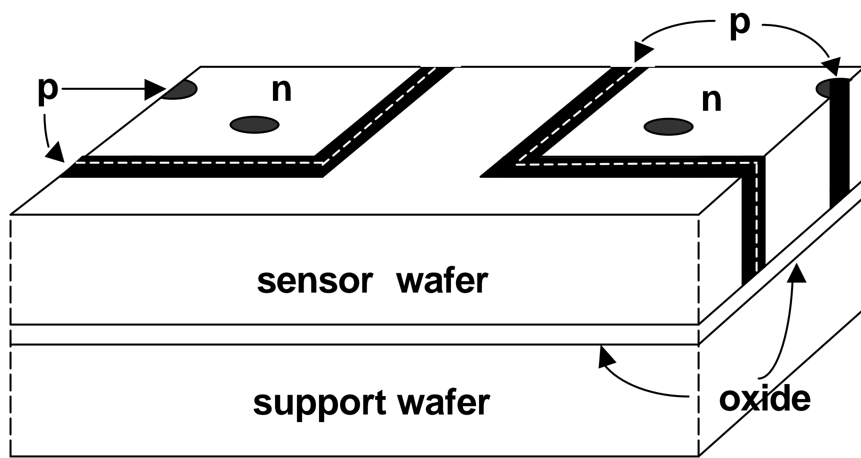
p
p
n
n
sensor wafer
support wafer
oxide

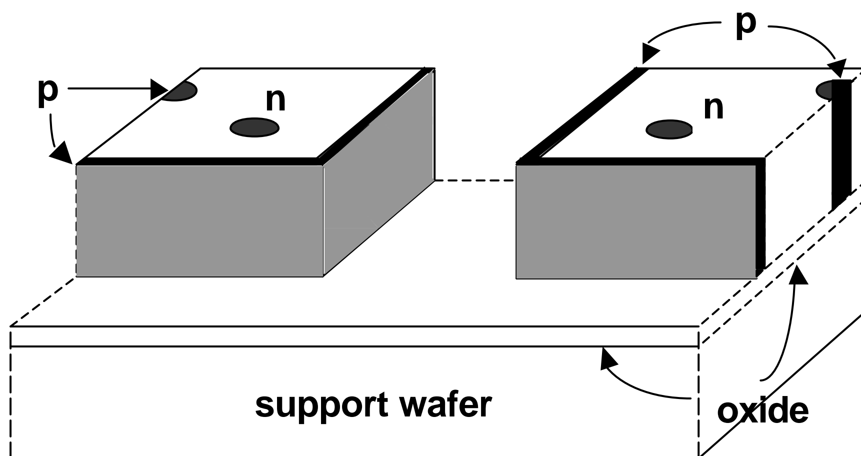
p
p
n
n
support wafer
oxide

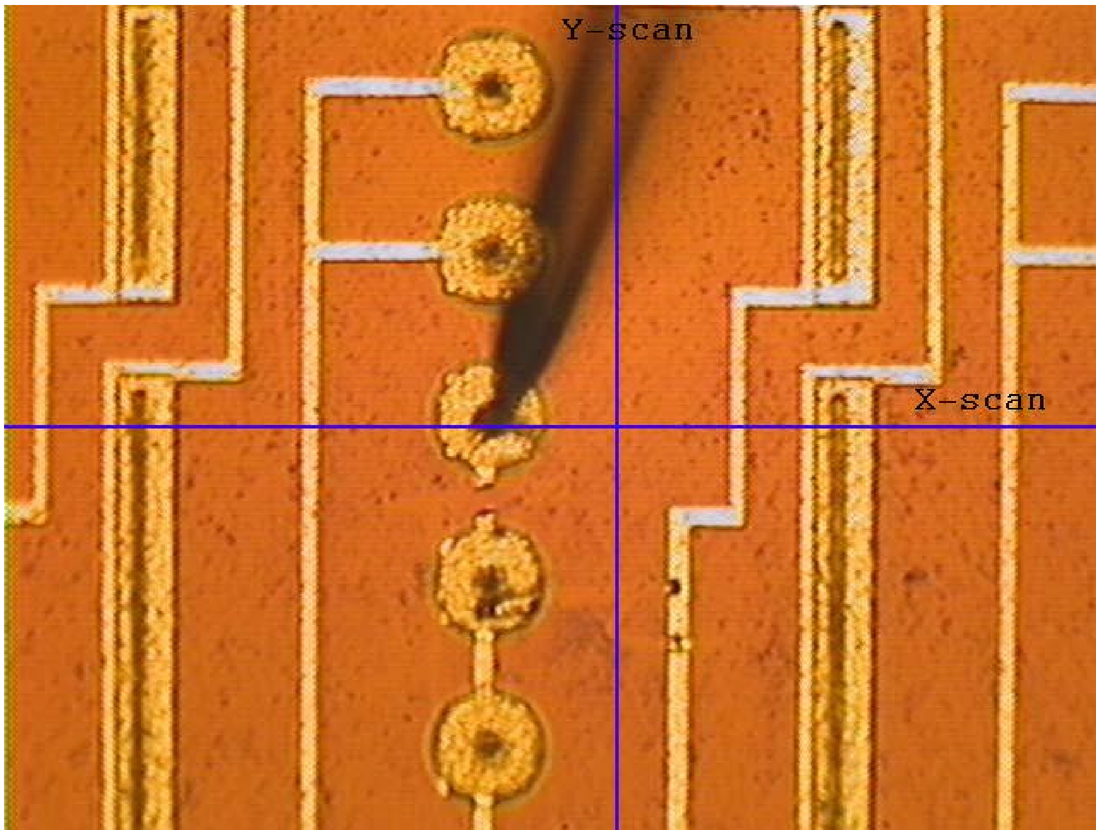
Y-scan
X-scan

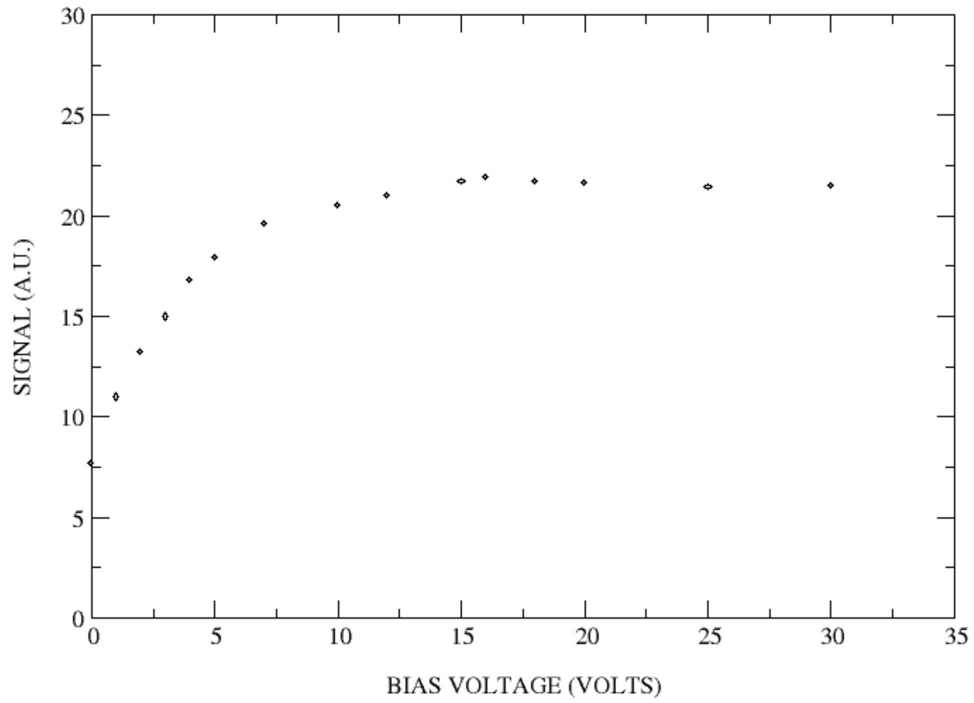
TRENCH SENSOR (12,10), STRIP OF P-ELECTRODES
INFRARED DIODE MICROBEAM
SIGNAL (A.U.)
BIAS VOLTAGE (VOLTS)
0
5
10
15
20
25
30
35

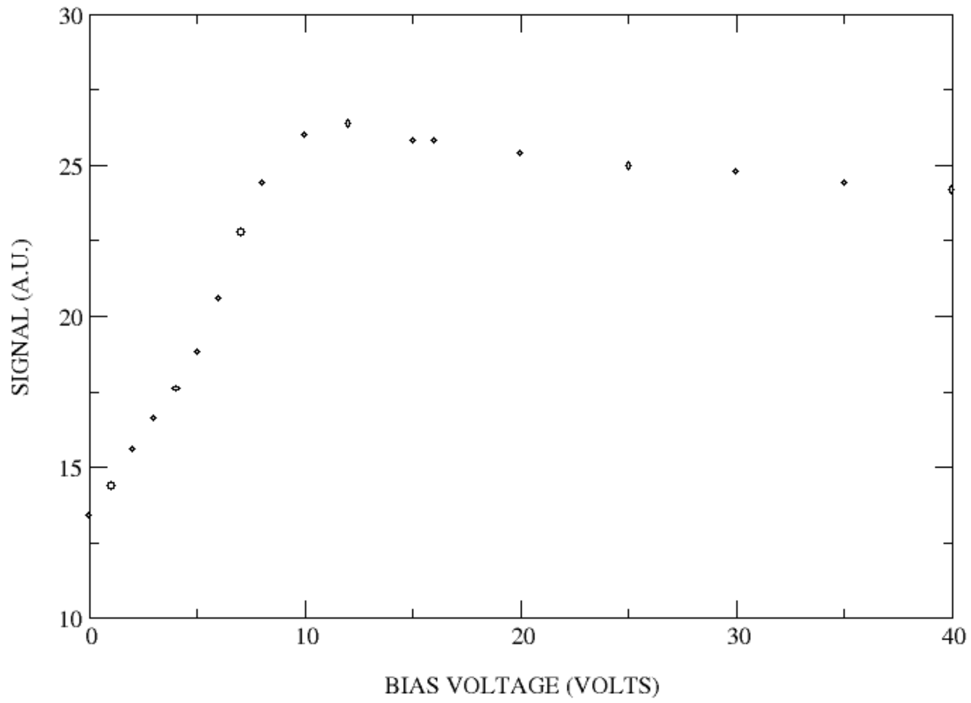
ACTIVE TRENCH - SINGLE ELECTRODE
SIGNAL (A.U.)
BIAS VOLTAGE (VOLTS)
30
25
20
15
10
0
10
20
30
40

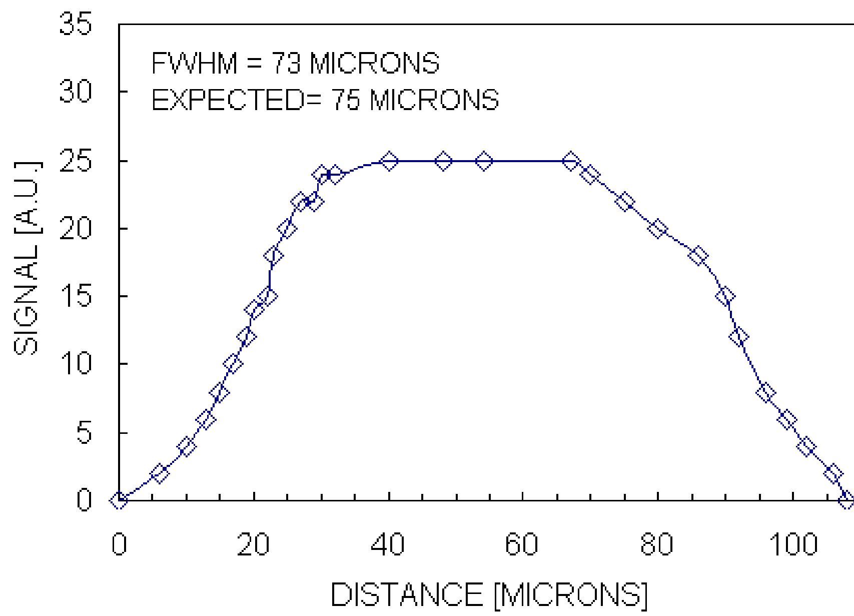
FWHM = 73 MICRONS
EXPECTED= 75 MICRONS
SIGNAL [A.U.]
DISTANCE [MICRONS]
35
30
25
20
15
10
5
0
0
20
40
60
80
100

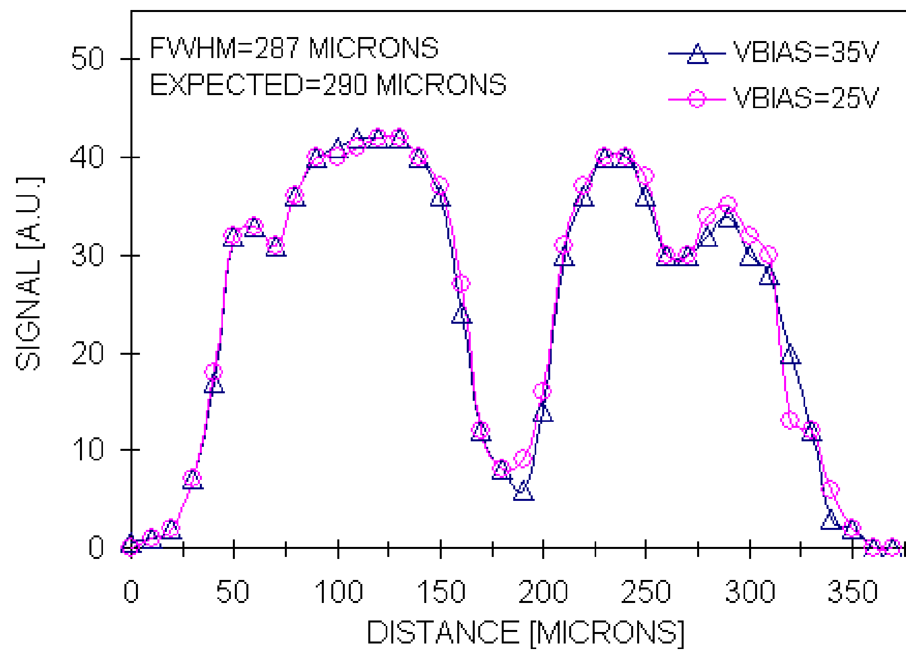
FWHM=287 MICRONS
EXPECTED=290 MICRONS
VBIAS=35V
VBIAS=25V
SIGNAL [A.U.]
DISTANCE [MICRONS]
0
10
20
30
40
50
0
50
100
150
200
250
300
350

Title:
Maple plot
Creator:
Maple
Preview:
This EPS picture was not saved
with a preview included in it.
Comment:
This EPS picture will print to a
PostScript printer, but not to
other types of printers.